Hindawi
Geofluids
Volume 2023, Article ID 4658604, 16 pages
https://doi.org/10.1155/2023/4658604

Research Article

Well-Testing Model for Dual-Porosity Reservoir considering Stress-Sensitivity and Elastic Outer Boundary Condition

Song Chol Kim,[1] **Song Guk Han**,[1] **Yong Il Song**,[1] **Jin Sim Kim**,[2] **and Myong Gun Hong**[1]

[1]*Faculty of Earth Science and Technology, Kim Chaek University of Technology, Pyongyang 999093, Democratic People's Republic of Korea*
[2]*International Technology Cooperation Center, Kim Chaek University of Technology, Pyongyang 999093, Democratic People's Republic of Korea*

Correspondence should be addressed to Song Chol Kim; ksc71821@star-co.net.kp

Received 22 March 2023; Revised 20 October 2023; Accepted 25 October 2023; Published 16 November 2023

Academic Editor: Amin Shokrollahi

Stress sensitivity and the elastic outer boundary (EOB) condition have a great effect on the analysis of the characteristics of the fluid flow in a reservoir. When researchers analyzed the characteristics of the fluid flow, they have considered the stress sensitivity and the EOB condition separately but have not considered them simultaneously. Therefore, errors are inevitable during the analysis of well testing. The main object of this work is to present a well-testing model for stress-sensitivity dual-porosity reservoir (DPR) with EOB to improve the accuracy of the analysis of well-testing data. To this end, in this paper, we established a well-testing model for the DPR, considering the stress sensitivity and the EOB simultaneously, and presented its semianalytical solution. On the basis of the consideration of the EOB condition and stress sensitivity of permeability (SSP), a seepage model for the DPR with the EOB is built using the continuity equation, motion equation, state equation, and interporosity flow equation between matrix and fracture, which considers the stress sensitivity, wellbore storage, and skin. To solve this model, a nonlinear partial differential equation is changed into a linear form of a partial differential equation by introducing an effective well radius and applying Pedrosa's transformation and perturbation transformation. Applying the Laplace transformation, an analytical solution in the Laplace space is obtained, and curves of pressure and pressure derivative (PPD) are drawn by numerically inverting them. The model is verified by comparing it with the EOB without consideration of SSP and using case data. The sensitivity of parameters on the curves of PPD is analyzed. This work may be significant for evaluating more accurately the parameters of wells and reservoirs using well testing.

1. Introduction

During the development of oil and gas reservoirs, pressure drops and effective stress increases, so their permeability changes. Stress sensitivity has an effect on accurately evaluating the characteristics of wells and reservoirs.

Many researchers have researched the stress sensitivity of reservoirs and established models considering it. Experimental researches on oil reservoirs and coalbed methane reservoirs were also carried out [1–10]. Their experiments determined the effect of the formation stress on the permeability and its relationship. In order to study the relationship between the compressibility of the pore-fracture system and its effective stress, Zhang et al. [11] conducted an experiment with the nuclear magnetic resonance technique, calculated the stress sensitivity of the pore and fracture, and discussed the variation of its heterogeneity. Based on many compaction researches of rocks, Chilingar et al. [12] argued that well testing could be wrong due to the plastic deformation that increases the effective stress in undercompacted overpressured reservoirs, and thus, many erroneously condemned overpressured reservoirs should be reexamined and reevaluated, and techniques should be developed to recover the oil and gas from these stress-sensitivity reservoirs. Guo et al.

[13] and Meng et al. [14] presented semianalytical models to evaluate production features in the stress-sensitivity carbonate gas reservoirs, which were considered triple-porosity media composed of matrix, fractures, and vugs. Aguilera [15] proposed a material-balance equation considering the effective compressibility of fractures and matrix, and Wang et al. [16, 17], Luo et al. [18], and Mo et al. [19] established the fluid flow model for the stress-sensitivity fracture reservoirs. Zhang et al. [20] suggested the well-testing model for the stress-sensitivity DPR, where its thickness and fluid property vary in the radial direction, and Tian et al. [21] presented the well-testing model for a multiregion radially composite reservoir considering the stress sensitivity. Ren and Guo [22] researched the general method for analyzing nonsteady flow, and Jelmert and Toverud [23] obtained the approximate analytical solution for stress-sensitivity deformable reservoirs and drew the corresponding type curve. Xia et al. [24] established the numerical model, considering nonlinear filter features, wellbore storage, and skin, and proposed the general method for evaluating the effect of fracture on the volume strain of a vertical well based on the well-testing and production data. Zhu and Liang [25] derived the production equation considering stress sensitivity and analyzed the effect of stress sensitivity on production. Moradi et al. [26] studied three-dimensional transient pressure features and pressure drop in the stress-sensitivity reservoirs during the production of hydrocarbons, and Zhu et al. [27] proposed the analytical model for stress-sensitivity coalbed methane reservoirs to study the permeability evolution during production. Based on a combination of geomechanics and flow characteristics, Li et al. [28] presented the production model for triple-porosity media, taking the adsorption and desorption of gas, slip flow, Knudsen, interfacial diffusions, and stress sensitivity into account. Chen et al. [29] established the mathematical model for tight gas reservoirs considering threshold pressure gradient, gas slipping, and stress sensitivity, and Xue et al. [30] conducted research on tight sandstone gas reservoirs with water produced and showed that strong stress sensitivity appeared as a result and increased with the water production. Zhao et al. [31], Jabbari et al. [32], Samaniego and Villalobos [33], and Zhang et al. [34] carried out research on the stress-sensitivity of fracture reservoirs, and Wang and Wang [35] proposed the mathematical model considering the effect of slipping and stress sensitivity in fractured gas reservoirs. Huang et al. [36] presented the transient flow model for horizontal wells in stress-sensitivity composite reservoirs, and Li et al. [37] presented the dual-porosity media model for horizontal wells in fractured tight gas reservoirs with stress sensitivity. Yuan et al. [38] suggested a general solution for oil flow, taking multiphase flow, the properties of stress-sensitivity reservoirs, and the changes in operation conditions into consideration. Li et al. [39] and Wang et al. [40] researched the characteristics of fluid flow in a stress-sensitivity tight reservoir, where they considered the reservoir as an outer unstimulated reservoir volume region and an inner stimulated reservoir volume region. Jiang and Yang [41] presented the fully coupled fluid flow and geomechanics model in fractured shale gas reservoirs, which characterized stress-sensitivity productivity, and Guo et al. [42] proposed transient pressure and decline rate analysis in shale gas reservoir, considering multiflow mechanics including desorption, diffusion, Darcy's flow, and stress sensitivity. Wu et al. [43], Xu et al. [44], Zhang and Yang [45, 46], and Zongxiao et al. [47] presented well-testing models for multifractured horizontal stress-sensitivity reservoirs. Wu et al. [48], Ji et al. [49], Huang et al. [50], and Wu et al. [51] established the well-testing models for the multifractured horizontal well in the stress-sensitivity tight reservoirs. Wang et al. [52], Liu et al. [53], and Du et al. [54] presented the well-testing models for the multifractured horizontal wells in the stress-sensitivity shale gas, and Chen et al. [55] and Wang et al. [56] presented the mathematical model of the transient pressure features in the stress-sensitivity coalbed methane reservoirs. Liu [57] discussed the well-testing model for multifractured horizontal wells, considering the effect of stress sensitivity and the threshold pressure gradient in a low-permeable reservoir. Zhang et al. [58] built the analytical well-testing model for a low-permeable reservoir with consideration of anisotropy, heterogeneity, stress sensitivity, wellbore storage, and skin, and Wang et al. [59] presented the analytical model for multilateral horizontal wells considering the combination of multiple branches and stress sensitivity in low-permeability natural fracture reservoirs. Cao et al. [60] and Yan et al. [61] researched the transient pressure behavior of wells, considering the effects of sand production and stress sensitivity simultaneously. Zhang and Tong [62] studied the transient pressure response of fractal media in stress-sensitive low-permeability reservoirs. Gao et al. [63] established a well-testing model of pressure buildup considering stress sensitivity and the hysteresis effect in deep-water composite reservoirs with high temperature and pressure. Shovkun and Espinoza [64] conducted the coupled fluid flow and geomechanics simulation for the coal and shale reservoirs with consideration of the impact of desorption-induced stress, shear failure, and fines migration. The well-testing models relevant to the stress sensitivity mentioned above have been considered only for reservoirs with ideal outer boundaries. However, there are few ideal outer boundaries in reality. Therefore, when the outer boundary is considered the ideal boundary, the reservoirs cannot be described objectively, and errors are inevitable.

SSP makes its heterogeneity stronger in heterogeneous reservoirs. Although such strong heterogeneity gives for detailed characterization of different aspects of the reservoir, it may be tedious and time-consuming in real application. In order to simply describe the stress-sensitivity reservoir, many researchers have introduced a conception of the permeability modulus to ensure the robustness of the analytical solution [20, 36, 40, 47, 48, 52, 58, 59].

Several researchers studied the fluid flow characteristics of the reservoirs with the EOB. Li et al. [65] studied the seepage model for the homogeneous reservoir by introducing the EOB, and Li et al. [66] discussed an elastic boundary value problem of the extended modified Bessel equation introducing the elastic boundary value condition, established the seepage model for fractal homogeneous reservoirs with the EOB, and obtained its solution. Kim et al. [67] built the well-testing model for the DPRs with the EOB

considering skin and wellbore storage and introducing effective well radius, and Zheng et al. [68] established the dual-porosity media seepage model for shale reservoirs with the EOB taking the adsorption and desorption processes into account. Zhao and Min [69] presented the non-Newtonian power-law fluid percolation model with the EOB. The stress sensitivity of the reservoir is not considered in the models with the EOB mentioned above.

Both stress sensitivity and the EOB condition significantly affect the characteristics of fluid flow in reservoirs, but stress sensitivity and the elastic boundary condition were not considered simultaneously in previous researches. The precedent researchers have considered either fluid flow in the stress-sensitivity reservoirs with the ideal boundary conditions or the elasticity of the boundary in the reservoirs without considering stress sensitivity. This affects the analysis of well-testing data and results in considerable errors.

In this paper, the well-testing model for DPR is established considering the stress sensitivity and EOB condition simultaneously, and its solution is obtained to improve the accuracy of the analysis of well-testing data. On the basis of the consideration of the EOB condition and SSP, the seepage model for the DPR with the EOB is built using the continuity equation, motion equation, state equation, and interporosity flow equation between matrix and fracture. By applying effective well radius, Pedrosa's transformation, perturbation transformation, and the Laplace transformation, an analytical solution in the Laplace space is obtained, and curves of PPD are drawn by numerically inverting them.

This work may be significant for evaluating more accurately the parameters of wells and reservoirs using well testing.

2. EOB Condition

Li et al. [65] defined an elastic coefficient of the reservoir as follows:

$$\varepsilon_r^P = \varepsilon_r^P(r,t) = \frac{\partial \ln P}{\partial \ln r} = \frac{r}{P}\frac{\partial P}{\partial r}, \tag{1}$$

$$P = p_i - p, \tag{2}$$

where ε_r^P is the rate of the relative change of the pressure difference P with respect to r. p is the function of time (t) and position (x, y, and z).

$$p = p(x,y,z,t), \tag{3}$$

The farther the distance from a well is, the lower the pressure difference is. Thus, the change direction of pressure difference is opposite to the change direction of the position.

Therefore, the elastic coefficient of the outer boundary in a cylinder reservoir can be defined as follows [67]:

$$\varepsilon_T^P = \varepsilon_T^{P_D} = \varepsilon_R^{P_D} = \varepsilon_{R_D}^{P_D} = -\left.\frac{\partial \ln P}{\partial \ln r}\right|_{r=R} = -\left.\frac{\partial \ln P_D}{\partial \ln r_D}\right|_{r_D=R_D}. \tag{4}$$

From Eq. (4), the EOB condition may be obtained as follows:

$$\left[\varepsilon_T^P P + r\frac{\partial P}{\partial r}\right]_{r=R} = 0, \tag{5}$$

or

$$\left[\varepsilon_T^{P_D} P_D + r_D\frac{\partial P_D}{\partial r_D}\right]_{r_D=R_D} = 0. \tag{6}$$

Equations (5) or (6) are elastic outer conditions.

3. Methodology

3.1. Physical Model

(1) Reservoir consists of the natural fracture and matrix, and fluid flows through both the natural fracture and matrix system. That is, the reservoir has dual porosity and dual permeability characteristics

(2) The permeability of the natural fracture system is considered stress sensitivity

(3) Reservoir has a uniform thickness of h

(4) Isotropic fluid flow in a single phase is assumed

(5) The effects of gravity and capillary are negligible

This physical model is suitable for matrix-fracture dual-porosity reservoirs, including naturally fractured carbonate reservoirs. This requires that the reservoir with a uniform thickness be on a horizontal plane.

3.2. Mathematical Model. Using the state equation, motion equation, interporosity flow equation, and continuity equation, a seepage differential equation for dual porosity reservoir considering the stress sensitivity is obtained. For convenience, the seepage model is nondimensionalized using dimensionless variables. The detailed derivation of the mathematical model is provided in Appendix A.

The seepage differential equation for the matrix system in the natural fracture reservoir is as follows.

$$\frac{\partial^2 p_m}{\partial r^2} + \frac{1}{r}\frac{\partial p_m}{\partial r} = \frac{\varphi_{mi}\mu C_{mt}}{k_m}\frac{\partial p_m}{\partial t} + \alpha\left(p_m - p_f\right). \tag{7}$$

The seepage differential equation for the natural fracture system in the natural fracture reservoir is as follows.

$$\frac{\partial^2 p_f}{\partial r^2} + \frac{1}{r}\frac{\partial p_f}{\partial r} + \gamma\left(\frac{\partial p_f}{\partial r}\right)^2 = e^{-\gamma\left(p_f - p_i\right)}\left[\frac{\varphi_{fi}\mu C_{\mathrm{ft}}}{k_{fi}}\frac{\partial p_f}{\partial t} - \frac{\alpha k_m}{k_{fi}}\left(p_m - p_f\right)\right]. \tag{8}$$

The initial condition is as follows:

$$p_f(r,t)\Big|_{t=0} = p_m(r,t)|_{t=0} = p_i. \tag{9}$$

The inner boundary condition is as follows:

$$C\frac{dp_w}{dt} - \left[\frac{2\pi rhk_{fi}e^{\gamma(p_f-p_i)}}{\mu}\left(\frac{\partial p_f}{\partial r}\right) + \frac{2\pi rhk_m}{\mu}\left(\frac{\partial p_m}{\partial r}\right)\right]_{r=r_w} = -qB, \tag{10}$$

$$p_w = \left(p_f - Sr\frac{\partial p_f}{\partial r}\right)\Big|_{r=r_w} = \left(p_m - Sr\frac{\partial p_m}{\partial r}\right)\Big|_{r=r_w}. \tag{11}$$

The outer boundary condition is as follows:

$$\left[\varepsilon_\Gamma^{P_f} p_f + r\frac{\partial p_f}{\partial r}\right]\Big|_{r=R} = \left[\varepsilon_\Gamma^{P_f} p_m + r\frac{\partial p_m}{\partial r}\right]\Big|_{r=R} = 0. \tag{12}$$

Introducing the dimensionless variables, Eqs. (7)~(12) are nondimensionalized, and these equations are arranged using $r_{De} = r_D e^S$ and $T_D = t_D/C_D$.

The dimensionless seepage differential equation for the natural fracture system in the natural fracture reservoir is as follows.

$$\begin{aligned}&\frac{\partial^2 p_{fD}}{\partial r_{De}^2} + \frac{1}{r_{De}}\frac{\partial p_{fD}}{\partial r_{De}} - \gamma_D\left[\frac{\partial p_{fD}}{\partial r_{De}}\right]^2 \\ &\quad = e^{\gamma_D p_{fD}}\left[\frac{\omega}{KC_D e^{2S}}\frac{\partial p_{fD}}{\partial T_D} + \frac{\lambda e^{-2S}}{K}\left(p_{fD} - p_{mD}\right)\right].\end{aligned} \tag{13}$$

The dimensionless seepage differential equation for the matrix system in the natural fracture reservoir is as follows.

$$\frac{\partial^2 p_{mD}}{\partial r_{De}^2} + \frac{1}{r_{De}}\frac{\partial p_{mD}}{\partial r_{De}} = \frac{1-\omega}{(1-K)C_D e^{2S}}\frac{\partial p_{mD}}{\partial T_D} + \frac{\lambda e^{-2S}}{1-K}\left(p_{mD} - p_{fD}\right). \tag{14}$$

The dimensionless initial condition is as follows:

$$p_{fD}(r_{De}, T_D)\Big|_{T_{D=0}} = p_{mD}(r_{De}, T_D)|_{T_{D=0}} = 0. \tag{15}$$

The dimensionless inner boundary condition is as follows:

$$\frac{dp_{wD}}{dT_D} - \left[Kr_{De}e^{\gamma_D p_{fD}}\frac{\partial p_{fD}}{\partial r_{De}} + (1-K)r_{De}\frac{\partial p_{mD}}{\partial r_{De}}\right]\Big|_{r_{De}=1} = 1, \tag{16}$$

$$p_{wD} = p_{fD}(1, T_D) = p_{mD}(1, T_D). \tag{17}$$

The dimensionless outer boundary condition is as follows:

$$\left[\varepsilon_\Gamma^{P_{fD}} p_{fD} + r_{De}\frac{\partial p_{fD}}{\partial r_{De}}\right]\Big|_{r_{De}=R_{De}} = \left[\varepsilon_\Gamma^{P_{fD}} p_{mD} + r_{De}\frac{\partial p_{mD}}{\partial r_{De}}\right]\Big|_{r_{De}=R_{De}} = 0. \tag{18}$$

3.3. Solution of Model. The seepage differential equation (Eq. (13)) for fracture system and inner boundary condition (Eq. (15)) have strong nonlinearity. Therefore, Pedrosa's transformation and perturbation transformation are applied so as to linearize these equations. Laplace transformation is applied to obtain its solution in the Laplace domain. The detailed derivation process is provided in Appendix B.

Applying Pedrosa's transformation, perturbation transformation, and the Laplace transformation, the following equations are obtained.

The seepage differential equation for natural fracture system is as follows:

$$\frac{\partial^2 \bar{\xi}_{fD0}}{\partial r_{De}^2} + \frac{1}{r_{De}}\frac{\partial \bar{\xi}_{fD0}}{\partial r_{De}} + A_1\bar{\xi}_{fD} + A_2\bar{p}_{mD} = 0. \tag{19}$$

The seepage differential equation for matrix system is as follows:

$$\left(\frac{\partial^2 \bar{p}_{mD}}{\partial r_{De}^2} + \frac{1}{r_{De}}\frac{\partial \bar{p}_{mD}}{\partial r_{De}}\right) + A_3\bar{p}_{mD} + A_4\bar{\xi}_{fD0} = 0. \tag{20}$$

The inner boundary condition is as follows:

$$z\bar{\xi}_{fD0}(1, T_D) - \left[Kr_{De}\frac{\partial \bar{\xi}_{fD0}}{\partial r_{De}} + (1-K)r_{De}\frac{\partial \bar{p}_{mD}}{\partial r_{De}}\right]\Big|_{r_{De}=1} = \frac{1}{z}, \tag{21}$$

$$\bar{\xi}_{wD0} = \bar{\xi}_{fD0}(1, T_D). \tag{22}$$

The outer boundary condition is as follows:

$$\left[\varepsilon_\Gamma^{P_{fD}}\bar{\xi}_{fD0} + r_{De}\frac{\partial \bar{\xi}_{fD0}}{\partial r_{De}}\right]\Big|_{r_{De}=R_{De}} = 0. \tag{23}$$

The special solutions to Eqs. (19) and (20) are obtained, and based on the special solutions, a general solution to Eqs. (19) and (20) is obtained. From the special solutions, the general solution to Eqs. (19) and (20) may be expressed as follows.

$$\bar{\xi}_{fD0} = A_f K_0\left(\sqrt{\sigma}r_{De}\right) + B_f I_0\left(\sqrt{\sigma}r_{De}\right), \tag{24}$$

where

$$\sigma = \frac{-(A_1 + A_3) - \sqrt{(A_1 - A_3)^2 + 4A_2A_3}}{2}. \tag{25}$$

Substituting the general solution Eq. (24) into the inner boundary condition (21) and outer boundary condition (23), the following equations are obtained.

$$C_1A_f + C_2B_f = \frac{1}{z}, \tag{26}$$

$$d_1 A_f + d_2 B_f = 0, \tag{27}$$

where

$$C_1 = zK_0\left(\sqrt{\sigma}\right) + \left[K + (1-K)\left(-\frac{\sigma + A_1}{A_2}\right)\right]\sqrt{\sigma}K_1\left(\sqrt{\sigma}\right), \tag{28}$$

$$C_2 = zI_0\left(\sqrt{\sigma}\right) - \left[K + (1-K)\left(-\frac{\sigma + A_1}{A_2}\right)\right]\sqrt{\sigma}I_1\left(\sqrt{\sigma}\right), \tag{29}$$

$$d_1 = \left[\varepsilon_\Gamma^{P_{fD}} K_0\left(\sqrt{\sigma}R_{De}\right) - R\sqrt{\sigma}K_1\left(\sqrt{\sigma}R_{De}\right)\right], \tag{30}$$

$$d_2 = \left[\varepsilon_\Gamma^{P_{fD}} I_0\left(\sqrt{\sigma}R_{De}\right) + R\sqrt{\sigma}I_1\left(\sqrt{\sigma}R_{De}\right)\right]. \tag{31}$$

From Eqs. (26) to (27), A_f and B_f are obtained as follows.

$$A_f = \frac{-d_2}{z(-c_1 d_2 + c_2 d_1)}, \tag{32}$$

$$B_f = \frac{d_1}{z(-c_1 d_2 + c_2 d_1)}. \tag{33}$$

From Eq. (22),

$$\bar{\xi}_{wD0} = \bar{\xi}_{fD0}(1, T_D) = A_f K_0\left(\sqrt{\sigma}\right) + B_f I_0\left(\sqrt{\sigma}\right). \tag{34}$$

ξ_{wD0} is obtained by numerically inverting the Laplace transformation (Eq. (34)). Many papers related to the well-testing model have used the Stehfest algorithm because of its simplicity and high accuracy. The algorithm proposed by Kim et al. [70] has lower numerical oscillation and higher accuracy than the Stehfest algorithm, and thus, this paper uses the algorithm proposed by Kim et al. [70], where $n = 25$, $a = 6.5$, $k = 2$, and $\sigma = 0$.

Bottom-hole PPD is calculated with the following equations.

$$p_{wD} = p_{fD}(1, T_D) = -\frac{1}{\gamma_D}\ln\left(1 - \gamma_D \xi_{wD0}\right), \tag{35}$$

$$T_D \frac{\partial p_{wD}}{\partial T_D} = -T_D \frac{\partial \xi_{wD0}}{\partial T_D} / (\gamma_D \xi_{wD0} - 1). \tag{36}$$

4. Results and Discussion

4.1. Verification of Model

4.1.1. Comparison Verification. To verify our model, it is compared to the model for the DPR with EOB without consideration of the stress sensitivity. When stress sensitivity is not considered in this model, as there is permeability modulus γ_D in the denominator of Eq. (35) and it converges into infinity, $\gamma_D \approx 0$(here, $\gamma_D = 10^{-10}$). Other parameters are as follows: $C_D = 100$, $S = 1$, $\omega = 10^{-5}$, and $\lambda = 10^{-4}$. $R_{De} = 2\,000$, $K = 0.999$, and $\varepsilon_\Gamma^{P_D} = 0, 0.1, 1\,000$. Figure 1 shows the result of comparison of the two models. The solid lines represent our model, and the circle marks the dual porosity without consideration of stress sensitivity [67]. From Figure 1, it can be seen that the two models agree well, which shows that our model is valid.

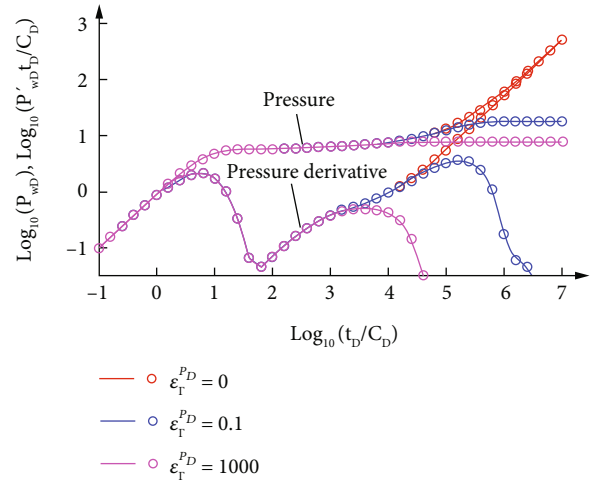

Figure 1: Result of comparison of our model to the model without consideration of stress sensitivity.

4.1.2. Verification Using Case Data. For verification, case data presented by Wang et al. [71] is used, which is obtained from an oil well in the Tahe oilfield. Figure 2 shows the result of matching with case data. As seen in Figure 2, the paper model agrees with the case data comparatively well, which shows that the model is valid. Analysis results are as follows: $k = 4.3\,\mu\text{m}^2$, $\omega = 0.041$, $\lambda = 1.825 \times 10^{-7}$, $S = -4.45$, $C = 0.205\,\text{m}^3/\text{MPa}$, $\gamma = 1.451\,\text{MPa}^{-1}$, $K = 0.999$, $R = 2\,100\,\text{m}$, and $\varepsilon_\Gamma^{P_D} = 0.5$.

4.2. Analysis of Sensitivity

4.2.1. Effect of Permeability Modulus γ_D on the PPD Curves. Figure 3 shows the effect of the permeability modulus γ_D ($\gamma_D = 0.001$, 0.01, 0.02, and 0.03) on the PPD curves. Other parameters are as follows: $C_D e^{2S} = 100$, $S = 1$, $\varepsilon_\Gamma^{P_D} = 100$, $\lambda = 10^{-3}$, $\omega = 10^{-5}$, $R_{De} = 2\,000$, and $K = 0.999$. As shown in Figure 3, the larger the value of γ_D, the higher the PPD curves. As time increases, the effect of the permeability modulus on PPD curves increases. When $\gamma_D \neq 0$, horizontal line of value 0.5 does not appear in the middle stage of the pressure derivative curve. This means that the SSP affects the analysis of the well-testing data.

4.2.2. Effect of Elastic Coefficient $\varepsilon_\Gamma^{P_D}$ of Outer Boundary on the PPD Curves. According to Li et al. [65], $\varepsilon_\Gamma^{P_D} \longrightarrow 0$ reflects the closed boundary, $\varepsilon_\Gamma^{P_D} \longrightarrow +\infty$ reflects the constant pressure boundary, $R_D \longrightarrow \infty$ reflects the infinite boundary, and $0 < \varepsilon_\Gamma^{P_D} < +\infty$ reflects between the closed boundary and constant pressure boundary.

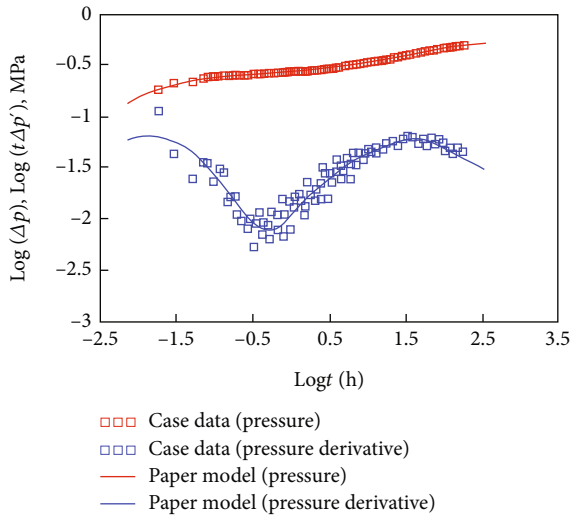

Figure 2: Result of matching with case data.

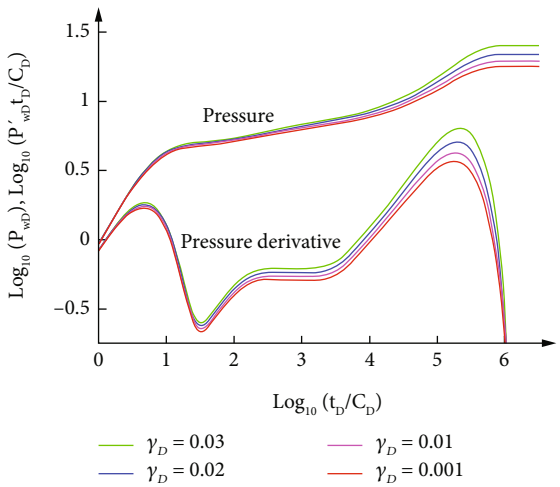

Figure 3: Effect of γ_D on the PPD curves.

Figure 4 shows the effect of the elastic coefficient $\varepsilon_\Gamma^{P_D}$ ($\varepsilon_\Gamma^{P_D} = 0$, 0.1, 1, and 1 000) of outer boundary on the PPD curves. Other parameters are as follows: $C_De^{2S} = 100$, $S = 1$, $\gamma_D = 0.01$, $\lambda = 10^{-3}$, $\omega = 10^{-5}$, $R_{De} = 2\,000$, and $K = 0.999$. As shown in Figure 4, $\varepsilon_\Gamma^{P_D}$ does not affect the early and middle stages of the pressure derivative curves but affects the late stage of the pressure derivative curves. When the value of $\varepsilon_\Gamma^{P_D}$ is zero, it reflects the closed boundary. While, when the value of $\varepsilon_\Gamma^{P_D}$ is 1 000, it reflects that is close to the closed boundary. Moreover, when $R_D \longrightarrow +\infty$, it reflects the infinite boundary. This means that with the value of $\varepsilon_\Gamma^{P_D}$, the late stage of PPD curves are between closed boundary and constant pressure boundary. The larger the value of $\varepsilon_\Gamma^{P_D}$increases, the higher the late stage of pressure curves gets from the horizontal line to the curve of the closed boundary and the higher the "hump" of the pressure derivative curve is. However, the outer boundary condition between the closed boundary and constant pressure boundary has not been considered in the model

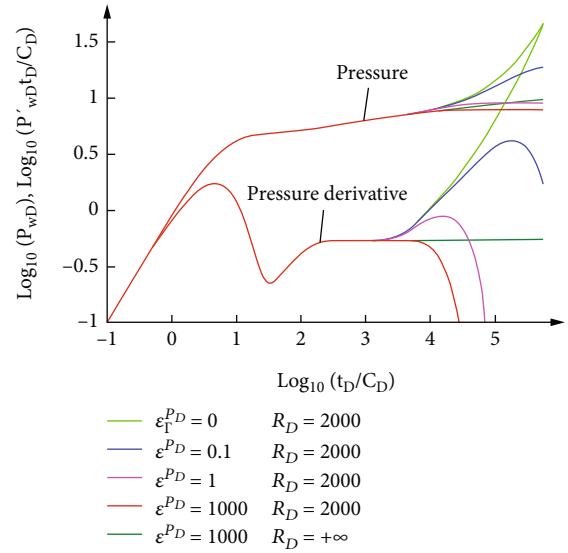

Figure 4: Effect of elastic coefficient $\varepsilon_\Gamma^{P_D}$ of outer boundary on the PPD curves.

of the reservoir with the ideal outer boundary (infinite boundary, closed boundary, and constant pressure boundary). Thus, our model has generality in comparison to the model with an ideal outer boundary. Therefore, this means that the accuracy of well-testing analysis can be enhanced.

4.2.3. Effect of C_De^{2S} on the PPD Curves. C_De^{2S} is a dimensionless quantity, which considers wellbore storage and skin simultaneously and shows degrees of improvement or damage to the well.

Figure 5 shows the effect of C_De^{2S} ($C_De^{2S} = 1\,000$, 2 000, 5 000, and 10 000) on the PPD curves. Other parameters are as follows: $S = 1$, $\gamma_D = 0.01$, $\varepsilon_\Gamma^{P_D} = 100$, $\lambda = 10^{-5}$, $\omega = 10^{-5}$, $R_{De} = 2\,000$, and $K = 0.999$. C_De^{2S} affects the middle stage of the pressure curve. The larger the value of C_De^{2S} increases, the higher the pressure derivative curves are in the middle stage and the earlier the effect of boundary appears on the pressure derivative curves.

4.2.4. Effect of Skin S on the PPD Curves. Figure 6 shows the effect of skin S ($S = -3$, -1, 0, 1, 3) on the PPD curves. Other parameters are as follows: $\gamma_D = 0.01$, $\varepsilon_\Gamma^{P_D} = 1$, $\lambda = 10^{-3}$, $\omega = 10^{-4}$, $C_De^{2S} = 10$, $R_D = 5\,000$, and $K = 0.999$. Skin S affects the middle and late stages of the PPD. The smaller value of S decreases, the upper the PPD curves are, the higher "hump" of the pressure derivative curve gets, and the later it appears.

4.2.5. Effect of Dimensionless Radius R_D on the PPD Curves. Figure 7 shows the effect of the dimensionless radius R_D ($R_D = 100$, 1 000, 5 000, 10 000) on the PPD curves. Other parameters are as follows: $\gamma_D = 0.01$, $\varepsilon_\Gamma^{P_D} = 1$, $\lambda = 10^{-3}$, $\omega = 10^{-5}$, $C_De^{2S} = 1\,000$, $S = 1$, and $K = 0.999$. R_D affects only the late stage of the PPD curves. The larger the value of R_D increases, the later the effect of boundary appears.

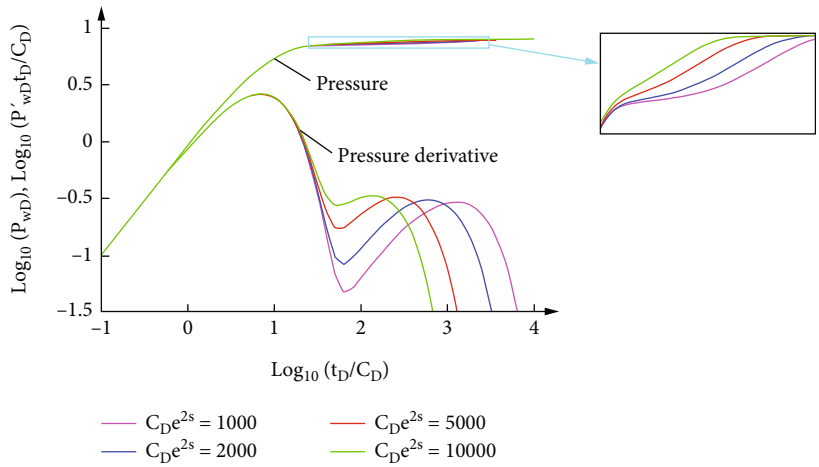

Figure 5: Effect of C_De^{2S} on the PPD curves.

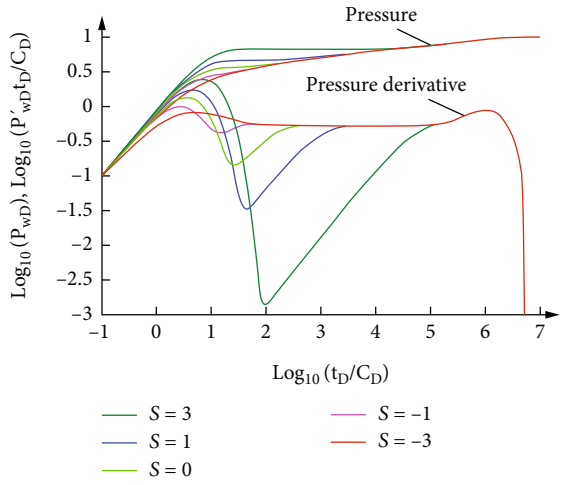

Figure 6: Effect of skin S on the PPD curves.

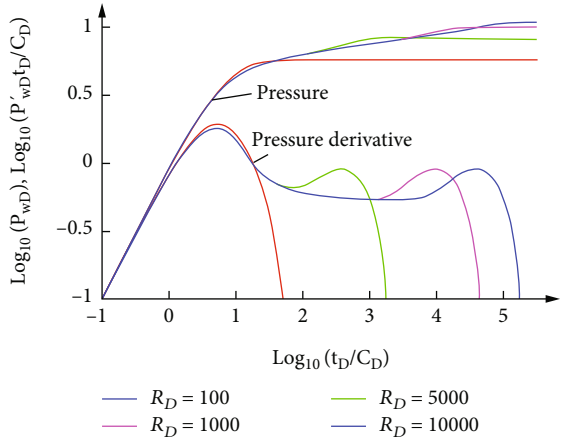

Figure 7: Effect of dimensionless radius R_D on the PPD curves.

4.2.6. Effect of Interporosity Flow Coefficient λ on the PPD Curves. Figure 8 shows the effect of the interporosity flow coefficient λ ($\lambda = 10^{-3}$, 10^{-4}, and 10^{-5}) on the PPD curves. Other parameters are as follows: $\gamma_D = 0.01$, $\varepsilon_T^{P_D} = 1$, $\omega = 10^{-4}$, $C_De^{2S} = 10$, $S = 1$, $R_D = 5\,000$, and $K = 0.999$. The interporosity flow coefficient λ affects the middle stage of the PPD curves. The larger the value of λ increases, the upper the PPD curves are, the higher the "hump" of the pressure derivative curve gets, the deeper the concave of the pressure derivative curve is, and the later the concave appears.

4.2.7. Effect of Storage Ratio ω on the PPD Curves. Figure 9 shows the effect of the storage ratio ω ($\omega = 10^{-1}$, 10^{-2}, and 10^{-3}) on the PPD curves. Other parameters are as follows: $\gamma_D = 0.01$, $\varepsilon_T^{P_D} = 1$, $\lambda = 10^{-4}$, $C_De^{2S} = 10$, $S = 1$, $R_D = 5\,000$, and $K = 0.999$. ω affects both the early and middle periods of flow. The smaller the value of ω gets, the upper the pressure curves are, the higher the "hump" of the pressure derivative curve gets, the deeper the concave is, and the earlier the concave appears.

4.2.8. Effect of Permeability Ratio K on the PPD Curves. Figure 10 shows the effect of the permeability ratio K ($K = 0.999$, 0.9, 0.85, and 0.8) on the PPD curves. Other parameters are as follows: $\gamma_D = 0.001$, $\varepsilon_T^{P_D} = 1$, $\omega = 10^{-4}$, $\lambda = 10^{-4}$, $C_De^{2S} = 1\,000$, $S = 0$, and $R_D = 500$. K affects both the early and middle periods of flow. The smaller the value of K, the upper the pressure curves are, and the higher the "hump" of the pressure derivative curve gets, the deeper the concave are.

Both the SSP and the condition of elasticity of the outer boundary greatly affect the well-testing analysis, but the previous papers have considered these effects individually and have not considered them simultaneously, which may result in considerable errors in the well-testing analysis. The well-testing model proposed in our paper considers the effect of the SSP and the condition of elasticity of the outer boundary simultaneously. Thus, this model may improve the accuracy of the well-testing analysis for the DPR. In reality, there is not only the dual-porosity reservoir for the vertical well but also the triple-porosity reservoir for the vertical well and the dual-porosity reservoir for the

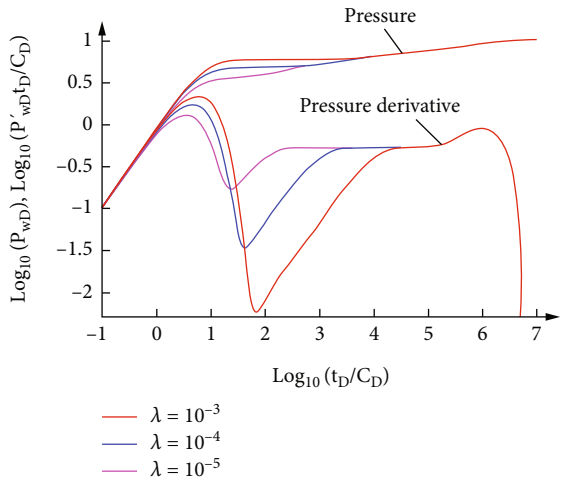

Figure 8: Effect of interporosity flow coefficient λ on the PPD curves.

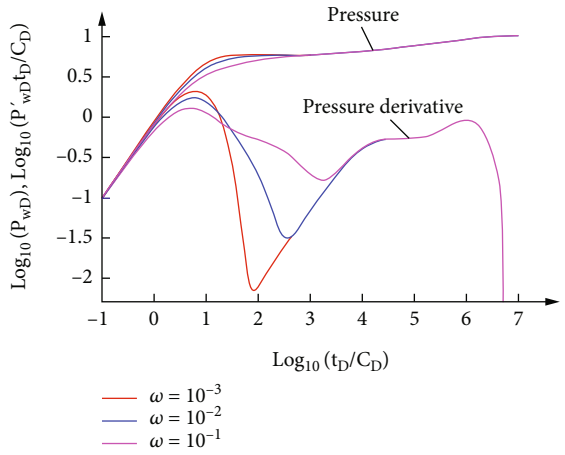

Figure 9: Effect of storage ratio ω on the PPD curves.

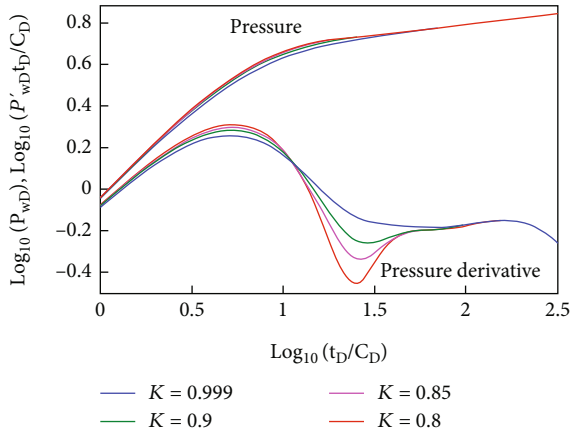

Figure 10: Effect of permeability ratio K on the PPD curves.

horizontal well. However, this model is limited to the dual-porosity model for vertical wells. The model proposed in this paper may be improved into dual-porosity and triple-porosity models for horizontal and inclined wells. We are going to study dual-porosity and the triple-porosity dual-permeability model for horizontal and inclined wells, considering stress sensitivity and EOB.

5. Conclusions

In this paper, the well-testing model for the DPR is presented, considering SSP and EOB simultaneously.

(1) The seepage differential equation for the DPR considering stress sensitivity and EOB simultaneously is established using the continuity equation, motion equation, state equation, and interporosity flow equation between matrix and fracture

(2) The dimensionless seepage differential equation is obtained using dimensionless variables

(3) Applying Pedrosa's transformation and perturbation transformation, the nonlinearity of the nonlinear seepage differential equation is decreased

(4) The analytical solution in the Laplace space is obtained by using the Laplace transformation, and the type curves of PPD are drawn by applying the Laplace numerical inversion [70]

(5) This model is verified by comparing it to the model in [67] with the EOB without consideration of SSP and using case data

(6) Through analysis of the sensitivity of parameters, it can be seen that both the SSP and EOB conditions affect the analysis of well-testing data

This model may improve the accuracy of the analysis of the well-testing data as compared with the previous well-testing model for DPR.

Appendix

A. Mathematical Model

In order to describe the degree of the SSP of the reservoir and its influence, Pedrosa [72] introduced the concept of a permeability modulus for the homogenous reservoir. As the reservoir pressure decreases, the opening of the natural fracture decreases. Therefore, the permeability of the natural fracture also decreases.

The permeability modulus is defined as follows:

$$\gamma = \frac{1}{k_f}\frac{dk_f}{dp_f}. \tag{A.1}$$

Integrating Eq. (A.1),

$$k_f = k_{fi}e^{-\gamma(p_i - p_f)}. \tag{A.2}$$

It is assumed that the fluid flows in the matrix and natural fracture system obey Darcy's law. The following equation may be obtained, which shows the fluid flow in a natural fracture.

$$v_f = \frac{k_f}{\mu}\frac{\partial p_f}{\partial r}. \tag{A.3}$$

Substituting Eq. (A.2) into Eq. (A.3),

$$v_f = \frac{k_{fi}e^{-\gamma\left(p_i-p_f\right)}}{\mu}\frac{\partial p_f}{\partial r}. \tag{A.4}$$

The motion equation of fluid flow in a matrix system is as follows.

$$v_m = \frac{k_m}{\mu}\frac{\partial p_m}{\partial r}. \tag{A.5}$$

To describe the changes in oil density in the natural fracture and matrix system during the production of oil, the following equations are applied, respectively.

$$\rho_f = \rho_o e^{C_o\left(p_f-p_i\right)}, \tag{A.6}$$

$$\rho_m = \rho_o e^{C_o\left(p_m-p_i\right)}. \tag{A.7}$$

To describe the changes in porosity of the natural fracture and matrix system during the production of oil, the following equations are applied, respectively.

$$\varphi_f = \varphi_{fi}e^{C_f\left(p_f-p_i\right)}, \tag{A.8}$$

$$\varphi_m = \varphi_{mi}e^{C_m\left(p_f-p_i\right)}. \tag{A.9}$$

It is assumed that the interporosity flow is pseudosteady state. Then, the following equation should be satisfied [73]:

$$q^* = \frac{\alpha k_m \rho_o}{\mu}\left(p_m - p_f\right). \tag{A.10}$$

The continuity equation of fluid flow in the natural fracture system may be obtained as follows:

$$\frac{1}{r}\frac{\partial\left(r\rho_f v_f\right)}{\partial r} = \frac{\partial\left(\rho_f\varphi_f\right)}{\partial t} - q^*. \tag{A.11}$$

The continuity equation of fluid flow in the matrix system may be obtained as follows:

$$\frac{1}{r}\frac{\partial(r\rho_m v_m)}{\partial r} = \frac{\partial(\rho_m\varphi_m)}{\partial t} + q^*. \tag{A.12}$$

In order to obtain a seepage differential equation for the matrix system, Eqs. (A.5), (A.7), (A.9), and (A.10) are substituted into Eq. (A.12).

$$\frac{\partial^2 p_m}{\partial r^2} + \frac{1}{r}\frac{\partial p_m}{\partial r} = \frac{\varphi_{mi}\mu C_{mt}}{k_m}\frac{\partial p_m}{\partial t} + \alpha\left(p_m - p_f\right). \tag{A.13}$$

Equation (A.13) is a seepage differential equation for the matrix system in the natural fracture reservoir.

In order to obtain a seepage differential equation for the natural fracture system, Eqs. (A.4), (A.6), (A.8), and (A.10) are substituted into (A.11).

$$\frac{\partial^2 p_f}{\partial r^2} + \frac{1}{r}\frac{\partial p_f}{\partial r} + \gamma\left(\frac{\partial p_f}{\partial r}\right)^2 = e^{-\gamma\left(p_f-p_i\right)}\left[\frac{\varphi_{fi}\mu C_{\mathrm{ft}}}{k_{fi}}\frac{\partial p_f}{\partial t} - \frac{\alpha k_m}{k_{fi}}\left(p_m - p_f\right)\right]. \tag{A.14}$$

Equation (A.14) is a seepage differential equation for the natural fracture system considering the SSP in the natural fracture reservoir.

The reservoir has uniform pressure at the initial stage of oil production. Therefore, the initial condition is as follows.

$$p_f(r,t)\Big|_{t=0} = p_m(r,t)|_{t=0} = p_i. \tag{A.15}$$

Inner boundary condition is as follows.

$$C\frac{dp_w}{dt} - \left[\frac{2\pi rhk_{fi}e^{\gamma\left(p_f-p_i\right)}}{\mu}\left(\frac{\partial p_f}{\partial r}\right) + \frac{2\pi rhk_m}{\mu}\left(\frac{\partial p_m}{\partial r}\right)\right]_{r=r_w} = -qB, \tag{A.16}$$

$$p_w = \left(p_f - Sr\frac{\partial p_f}{\partial r}\right)\Big|_{r=r_w} = \left(p_m - Sr\frac{\partial p_m}{\partial r}\right)\Big|_{r=r_w}. \tag{A.17}$$

Considering the outer boundary as the elastic boundary, the outer boundary condition can be obtained as follows.

$$\left[\varepsilon_\Gamma^{P_f} p_f + r\frac{\partial p_f}{\partial r}\right]\Big|_{r=R} = \left[\varepsilon_\Gamma^{P_f} p_m + r\frac{\partial p_m}{\partial r}\right]\Big|_{r=R} = 0. \tag{A.18}$$

For convenience, the following dimensionless variables are defined.

The dimensionless pressure is $p_D = (2\pi(k_{fi}+k_m)h/qB\mu)\Delta p$ $(\Delta p = p_i - p)$.

The storage ratio is $\omega = \varphi_{fi}C_{\mathrm{ft}}/\varphi_{fi}C_{\mathrm{ft}} + \varphi_{mi}C_{mt}$.

The dimensionless interporosity flow coefficient is $\lambda = \alpha(k_m/k_{fi})r_w^2$.

The dimensionless time is $t_D = (k_{fi}+k_m)t/(\varphi_{fi}C_{\mathrm{ft}} + \varphi_{mi}C_{mt})\mu r_w^2$.

The dimensionless wellbore storage is $C_D = C/2\pi(\varphi_{fi}C_{\mathrm{ft}} + \varphi_{mi}C_{mt})hr_w^2$.

The dimensionless permeability modulus is $\gamma_D = (qB\mu/2\pi k_{fi}h)\gamma$.

Permeability ratio of fracture system to the sum of fracture and matrix system

$$K = \frac{k_{fi}}{(k_{fi} + k_m)}. \tag{A.19}$$

Introducing these dimensionless variables, the dimensionless equations can be obtained from Eqs. (A.13)~(A.18).

The dimensionless seepage differential equations for the natural fracture system and matrix system in the natural fracture reservoir are as follows.

$$K\left[\frac{\partial^2 p_{fD}}{\partial r_D^2} + \frac{1}{r_D}\frac{\partial p_{fD}}{\partial r_D} - \gamma_D\left(\frac{\partial p_{fD}}{\partial r_D}\right)^2\right] = e^{\gamma_D p_{fD}}\left[\omega\frac{\partial p_{fD}}{\partial t_D} + \lambda\left(p_{fD} - p_{mD}\right)\right], \tag{A.20}$$

$$(1-K)\left(\frac{\partial^2 p_{mD}}{\partial r_D^2} + \frac{1}{r_D}\frac{\partial p_{mD}}{\partial r_D}\right) = (1-\omega)\frac{\partial p_{mD}}{\partial t_D} + \lambda\left(p_{mD} - p_{fD}\right). \tag{A.21}$$

Dimensionless initial condition:

$$p_{fD}(r_D, t_D)\Big|_{t_{D=0}} = p_{mD}(r_D, t_D)|_{t_{D=0}} = 0. \tag{A.22}$$

Dimensionless inner boundary condition

$$C_D\frac{dp_{wD}}{dt_D} - \left[Kr_D e^{\gamma_D p_{fD}}\frac{\partial p_{fD}}{\partial r_D} + (1-K)r_D\frac{\partial p_{mD}}{\partial r_D}\right]\Bigg|_{r_D=1} = 1, \tag{A.23}$$

$$p_{wD} = \left(p_{fD} - S\frac{\partial p_{fD}}{\partial r_D}\right)\Bigg|_{r_D=1} = \left(p_{mD} - S\frac{\partial p_{mD}}{\partial r_D}\right)\Bigg|_{r_D=1}. \tag{A.24}$$

Dimensionless outer boundary condition:

$$\left[\varepsilon_\Gamma^{P_{fD}} p_{fD} + r_D\frac{\partial p_{fD}}{\partial r_D}\right]\Bigg|_{r_D=R_D} = \left[\varepsilon_\Gamma^{P_{fD}} p_{mD} + r_D\frac{\partial p_{mD}}{\partial r_D}\right]\Bigg|_{r_D=R_D} = 0. \tag{A.25}$$

The dimensionless well radius is introduced as follows:

$$r_{De} = r_D e^S. \tag{A.26}$$

Taking $T_D = t_D/C_D$, the dimensionless seepage differential equations for the natural fracture system and matrix system in the natural fracture reservoir can be written as follows.

$$\frac{\partial^2 p_{fD}}{\partial r_{De}^2} + \frac{1}{r_{De}}\frac{\partial p_{fD}}{\partial r_{De}} - \gamma_D\left[\frac{\partial p_{fD}}{\partial r_{De}}\right]^2 = e^{\gamma_D p_{fD}} \cdot \left[\frac{\omega}{KC_D e^{2S}}\frac{\partial p_{fD}}{\partial T_D} + \frac{\lambda e^{-2S}}{K}\left(p_{fD} - p_{mD}\right)\right], \tag{A.27}$$

$$\frac{\partial^2 p_{mD}}{\partial r_{De}^2} + \frac{1}{r_{De}}\frac{\partial p_{mD}}{\partial r_{De}} = \frac{1-\omega}{(1-K)C_D e^{2S}}\frac{\partial p_{mD}}{\partial T_D} + \frac{\lambda e^{-2S}}{1-K}\left(p_{mD} - p_{fD}\right). \tag{A.28}$$

Dimensionless initial condition:

$$p_{fD}(r_D, T_D)\Big|_{T_{D=0}} = p_{mD}(r_D, T_D)|_{T_{D=0}} = 0. \tag{A.29}$$

Dimensionless inner boundary condition:

$$\frac{dp_{wD}}{dT_D} - \left[Kr_{De}e^{\gamma_D p_{fD}}\frac{\partial p_{fD}}{\partial r_{De}} + (1-K)r_{De}\frac{\partial p_{mD}}{\partial r_{De}}\right]\Bigg|_{r_{De}=1} = 1, \tag{A.30}$$

$$p_{wD} = p_{fD}(1, T_D) = p_{mD}(1, T_D). \tag{A.31}$$

Dimensionless outer boundary condition

$$\left[\varepsilon_\Gamma^{P_{fD}} p_{fD} + r_{De}\frac{\partial p_{fD}}{\partial r_{De}}\right]\Bigg|_{r_{De}=R_{De}} = \left[\varepsilon_\Gamma^{P_{fD}} p_{mD} + r_{De}\frac{\partial p_{mD}}{\partial r_{De}}\right]\Bigg|_{r_{De}=R_{De}} = 0, \tag{A.32}$$

where $R_{De} = R_D e^S$.

B. Solution of Model

The seepage differential equation (Eq. (A.27)) for the fracture system and inner boundary condition (Eq. (A.30)) has strong nonlinearity. Therefore, to linearize these equations, Pedrosa's transformation and perturbation transformation are applied.

Pedrosa's transformation is as follows [72]:

$$p_{fD}(r_{De}, T_D) = -\frac{1}{\gamma_D}\ln\left(1 - \gamma_D\xi_{fD}\right). \tag{B.1}$$

Applying Pedrosa's transformation to Eqs. (A.27) and (A.29) and rearranging, the following equations are obtained.

The seepage differential equations for the natural fracture and matrix system in the natural fracture reservoir are as follows.

$$\frac{\partial^2 \xi_{fD}}{\partial r_{De}^2} + \frac{1}{r_{De}}\frac{\partial \xi_{fD}}{\partial r_{De}} = \frac{1}{(1-\gamma_D\xi_{fD})}\frac{\omega}{KC_D e^{2S}}\frac{\partial \xi_{fD}}{\partial T_D} + \frac{\lambda e^{-2S}}{K}\left\{\left[-\frac{1}{\gamma_D}\ln\left(1-\gamma_D\xi_{fD}\right)\right] - p_{mD}\right\}, \tag{B.2}$$

$$\frac{\partial^2 p_{mD}}{\partial r_{De}^2}+\frac{1}{r_{De}}\frac{\partial p_{mD}}{\partial r_{De}}=\frac{1-\omega}{(1-K)C_D e^{2S}}\frac{\partial p_{mD}}{\partial T_D}+\frac{\lambda e^{-2S}}{1-K}\cdot\left\{p_{mD}-\left[-\frac{1}{\gamma_D}\ln\left(1-\gamma_D\xi_{fD}\right)\right]\right\}. \tag{B.3}$$

Initial condition:

$$\xi_{fD}(r_{De},T_D)\big|_{T_{D=0}}=p_{mD}(r_{De},T_D)\big|_{T_{D=0}}=0. \tag{B.4}$$

Inner boundary condition:

$$\frac{1}{(1-\gamma_D\xi_{fD})}\frac{d\xi_{wD}}{dT_D}-\left[\frac{1}{(1-\gamma_D\xi_{fD})^2}Kr_{De}\frac{\partial\xi_{fD}}{\partial r_{De}}+(1-K)r_{De}\frac{\partial p_{mD}}{\partial r_{De}}\right]\Bigg|_{r_{De}=1}=1, \tag{B.5}$$

$$\xi_{wD}=\xi_{fD}(1,T_D)=\xi_{mD}(1,T_D). \tag{B.6}$$

Outer boundary condition:

$$\left[-\frac{\varepsilon_\Gamma^{P_{fD}}}{\gamma_D}\ln\left(1-\gamma_D\xi_{fD}\right)+\frac{1}{1-\gamma_D\xi_{fD}}r_{De}\frac{\partial\xi_{fD}}{\partial r_{De}}\right]\Bigg|_{r_{De}=R_{De}}=0. \tag{B.7}$$

The perturbation transformations are as follows [72]:

$$\xi_{fD}=\xi_{fD0}+\gamma_D\xi_{fD1}+\gamma_D^2\xi_{fD2}+\cdots\approx\xi_{fD0}, \tag{B.8}$$

$$-\frac{1}{\gamma_D}\ln\left[1-\gamma_D\xi_{fD}\right]=\xi_{fD}+\frac{1}{2}\gamma_D\xi_{fD}^2+\cdots\approx\xi_{fD}, \tag{B.9}$$

$$\frac{1}{1-\gamma_D\xi_{fD}}=1+\gamma_D\xi_{fD}+\gamma_D^2\xi_{fD}^2+\cdots\approx 1. \tag{B.10}$$

As the value of γ_D is very small ($\gamma_D<<1$), the solution of zero-order perturbation can satisfy the accuracy requirement. Thus, seepage differential equations, initial conditions, and inner and outer boundary conditions are written as follows.

Seepage differential equation for natural fracture system:

$$\frac{\partial^2\xi_{fD0}}{\partial r_{De}^2}+\frac{1}{r_{De}}\frac{\partial\xi_{fD0}}{\partial r_{De}}=\frac{\omega}{KC_De^{2S}}\frac{\partial\xi_{fD0}}{\partial T_D}+\frac{\lambda e^{-2S}}{K}\left(\xi_{fD0}-p_{mD}\right). \tag{B.11}$$

Seepage differential equation for matrix system:

$$\frac{\partial^2 p_{mD}}{\partial r_{De}^2}+\frac{1}{r_{De}}\frac{\partial p_{mD}}{\partial r_{De}}=\frac{1-\omega}{(1-K)C_De^{2S}}\frac{\partial p_{mD}}{\partial T_D}+\frac{\lambda e^{-2S}}{1-K}\left(p_{mD}-\xi_{fD0}\right). \tag{B.12}$$

Initial condition:

$$\xi_{fD0}(r_{De},T_D)\big|_{T_{D=0}}=p_{mD}(r_{De},T_D)\big|_{T_{D=0}}=0. \tag{B.13}$$

Inner boundary condition:

$$\frac{d\xi_{wD0}}{dT_D}-\left(r_{De}\frac{\partial\xi_{fD0}}{\partial r_{De}}+r_{De}\frac{\partial p_{mD}}{\partial r_{De}}\right)\Bigg|_{r_{De}=1}=1,, \tag{B.14}$$

$$\xi_{wD0}=\xi_{fD0}(1,T_D)=\xi_{mD}(1,T_D). \tag{B.15}$$

Outer boundary condition:

$$\left[\varepsilon_\Gamma^{P_{fD}}\xi_{fD0}+r_{De}\frac{\partial\xi_{fD0}}{\partial r_{De}}\right]\Bigg|_{r_{De}=R_{De}}=0. \tag{B.16}$$

The Laplace transformations are defined as follows:

$$\bar{\xi}_{fD0}(r_{De},z)=\int_0^\infty e^{-zT_D}\xi_{fD0}(r_{De},T_D)dT_D, \tag{B.17}$$

$$\bar{p}_{mD}(r_{De},z)=\int_0^\infty e^{-zT_D}p_{mD}(r_{De},T_D)dT_D. \tag{B.18}$$

The Laplace transformations of Eqs. (B.11)~(B.16) are taken with respect to T_D.

The equations for the natural fracture and matrix system in the Laplace space can be written as follows.

$$\frac{\partial^2\bar{\xi}_{fD0}}{\partial r_{De}^2}+\frac{1}{r_{De}}\frac{\partial\bar{\xi}_{fD0}}{\partial r_{De}}+A_1\bar{\xi}_{fD}+A_2\bar{p}_{mD}=0, \tag{B.19}$$

$$\left(\frac{\partial^2\bar{p}_{mD}}{\partial r_{De}^2}+\frac{1}{r_{De}}\frac{\partial\bar{p}_{mD}}{\partial r_{De}}\right)+A_3\bar{p}_{mD}+A_4\bar{\xi}_{fD0}=0. \tag{B.20}$$

Inner boundary condition in the Laplace space is as follows.

$$z\bar{\xi}_{fD0}(1,T_D)-\left[Kr_{De}\frac{\partial\bar{\xi}_{fD0}}{\partial r_{De}}+(1-K)r_{De}\frac{\partial\bar{p}_{mD}}{\partial r_{De}}\right]\Bigg|_{r_{De}=1}=\frac{1}{z}, \tag{B.21}$$

$$\bar{\xi}_{wD0}=\bar{\xi}_{fD0}(1,T_D). \tag{B.22}$$

Outer boundary condition in the Laplace space is as follows.

$$\left[\varepsilon_\Gamma^{P_{fD}}\bar{\xi}_{fD0}+r_{De}\frac{\partial\bar{\xi}_{fD0}}{\partial r_{De}}\right]\Bigg|_{r_{De}=R_{De}}=0. \tag{B.23}$$

where A_1 = -$((\omega/KC_De^{2S})z+(\lambda e^{-2S}/K))$, $A_2=\lambda e^{-2S}/K$, $A_3=-[(1-\omega/(1-K)C_De^{2S})z+(\lambda e^{-2S}/1-K)]$, and $A_4=(\lambda e^{-2S}/1-K)$.

The special solutions of Eqs. (B.19) and (B.20) may be expressed by $y_1=AK_0(\sqrt{\sigma}r)$ and $y_2=BI_0(\sqrt{\sigma}r)$. Using

these special solutions, σ and coefficients A and B may be obtained.

Substituting $\bar{\xi}_{fD0} = A_f K_0(\sqrt{\sigma} r)$ and $\bar{p}_{mD} = A_m K_0(\sqrt{\sigma} r)$ into Eqs. (B.19) and (B.20) and arranging

$$A_f \sigma + A_1 A_f + A_2 A_m = 0, \tag{B.24}$$

$$A_m \sigma + A_3 A_m + A_4 A_f = 0. \tag{B.25}$$

From Eqs. (B.24) to (B.25), the following equations are obtained.

$$A_m = -\frac{\sigma + A_1}{A_2} A_f, \quad A_m = -\frac{A_4}{\sigma + A_3} A_f, \tag{B.26}$$

$$\sigma_{1,2} = \frac{-(A_1 + A_3) \pm \sqrt{(A_1 - A_3)^2 + 4A_2 A_3}}{2}. \tag{B.27}$$

Substituting $\bar{\xi}_{fD0} = B_f I_0(\sqrt{\sigma} r)$ and $\bar{p}_{mD} = B_m I_0(\sqrt{\sigma} r)$ into Eqs. (B.19) and (B.20), the above results are also obtained.

From the special solutions, the general solution to Eqs. (B.19) and (B.20) may be expressed as follows.

$$\bar{\xi}_{fD0} = A_f K_0\left(\sqrt{\sigma} r\right) + B_f I_0\left(\sqrt{\sigma} r\right). \tag{B.28}$$

Taking $A_m = -(\sigma + A_1/A_2)A_f$, $B_m = -(\sigma + A_1/A_2)B_f$, and $\sigma = -(A_1 + A_3) - \sqrt{(A_1 - A_3)^2 + 4A_2 A_3}/2$ and substituting the general solution (B.28) into the inner boundary condition (B.21), the following equation is obtained.

$$z\left[A_f K_0\left(\sqrt{\sigma}\right) + B_f I_0\left(\sqrt{\sigma}\right)\right] - \left[-A_f K \sqrt{\sigma} K_1\left(\sqrt{\sigma}\right) + B_f K \sqrt{\sigma} I_1\left(\sqrt{\sigma}\right) - A_f (1 - K)\left(-\frac{\sigma + A_1}{A_2}\right)\sqrt{\sigma} K_1\left(\sqrt{\sigma}\right) + B_f (1 - K) \cdot \left(-\frac{\sigma + A_1}{A_2}\right)\sqrt{\sigma} I_1\left(\sqrt{\sigma}\right)\right] = \frac{1}{z}, \tag{B.29}$$

$$A_f\left\{z K_0\left(\sqrt{\sigma}\right) + \left[K + (1 - K)\left(-\frac{\sigma + A_1}{A_2}\right)\right]\sqrt{\sigma} K_1\left(\sqrt{\sigma}\right)\right\} + B_f\left\{z I_0\left(\sqrt{\sigma}\right) - \left[K + (1 - K)\left(-\frac{\sigma + A_1}{A_2}\right)\right]\sqrt{\sigma} I_1\left(\sqrt{\sigma}\right)\right\} = \frac{1}{z}. \tag{B.30}$$

Taking $A_m = -(\sigma + A_1/A_2)A_f$, $B_m = -(\sigma + A_1/A_2)B_f$, and $\sigma = -(A_1 + A_3) - \sqrt{(A_1 - A_3)^2 + 4A_2 A_3}/2$ and substituting the general solution (B.28) into the outer boundary condition (B.23), the following equation is obtained.

$$\varepsilon_\Gamma^{P_{fD}}\left[A_f K_0\left(\sqrt{\sigma} R_{De}\right) + B_f I_0\left(\sqrt{\sigma} R_{De}\right)\right] + A_f R_{De}\left(-\sqrt{\sigma}\right) K_1\left(\sqrt{\sigma} R_{De}\right) + B_f R_{De} \sqrt{\sigma} I_1\left(\sqrt{\sigma} R_{De}\right) = 0, \tag{B.31}$$

$$A_f\left[\varepsilon_\Gamma^{P_{fD}} K_0\left(\sqrt{\sigma} R_{De}\right) - R_{De} \sqrt{\sigma} K_1\left(\sqrt{\sigma} R_{De}\right)\right] + B_f\left[\varepsilon_\Gamma^{P_{fD}} I_0\left(\sqrt{\sigma} R_{De}\right) + R_{De} \sqrt{\sigma} I_1\left(\sqrt{\sigma} R_{De}\right)\right] = 0. \tag{B.32}$$

Eqs. (B.30) and (B.32) are rewritten.

$$C_1 A_f + C_2 B_f = \frac{1}{z}, \tag{B.33}$$

$$d_1 A_f + d_2 B_f = 0, \tag{B.34}$$

where

$$C_1 = z K_0\left(\sqrt{\sigma}\right) + \left[K + (1 - K)\left(-\frac{\sigma + A_1}{A_2}\right)\right]\sqrt{\sigma} K_1\left(\sqrt{\sigma}\right), \tag{B.35}$$

$$C_2 = z I_0\left(\sqrt{\sigma}\right) - \left[K + (1 - K)\left(-\frac{\sigma + A_1}{A_2}\right)\right]\sqrt{\sigma} I_1\left(\sqrt{\sigma}\right), \tag{B.36}$$

$$d_1 = \left[\varepsilon_\Gamma^{P_{fD}} K_0\left(\sqrt{\sigma} R_{De}\right) - R_{De} \sqrt{\sigma} K_1\left(\sqrt{\sigma} R_{De}\right)\right], \tag{B.37}$$

$$d_2 = \left[\varepsilon_\Gamma^{P_{fD}} I_0\left(\sqrt{\sigma} R_{De}\right) + R_{De} \sqrt{\sigma} I_1\left(\sqrt{\sigma} R_{De}\right)\right]. \tag{B.38}$$

From (B.33) to (B.34), A_f and B_f are obtained as follows.

$$A_f = \frac{-d_2}{z(-c_1 d_2 + c_2 d_1)}, \tag{B.39}$$

$$B_f = \frac{d_1}{z(-c_1 d_2 + c_2 d_1)}. \tag{B.40}$$

From Eq. (B.22),

$$\bar{\xi}_{wD0} = \bar{\xi}_{fD0}(1, T_D) = A_f K_0\left(\sqrt{\sigma}\right) + B_f I_0\left(\sqrt{\sigma}\right). \tag{B.41}$$

Nomenclature

B: Volume factor, dimensionless
C: Wellbore storage coefficient, m^3/Pa
C_D: Dimensionless wellbore storage, dimensionless

C_m, C_f: Compressibility of matrix and natural fracture system, respectively, Pa^{-1}
C_{mt}: Total compressibility of matrix system and oil, $C_{mt} = C_m + \varphi_m C_o$, Pa^{-1}
C_{ft}: Total compressibility of natural fracture system and oil, $C_{ft} = C_f + \varphi_f C_o$, Pa^{-1}
C_o: Oil compressibility, Pa^{-1}
K: Permeability ratio of fracture system to the sum of fracture and matrix system, fraction
k_m, k_f: Permeability of matrix and natural fracture system, respectively, m^2
k_{fi}: Permeability of natural fracture under initial condition, m^2
h: Reservoir thickness, m
p: Reservoir pressure, Pa
R: Outer boundary radius, m
R_D: Dimensionless outer boundary radius, dimensionless
p_m, p_f: Pressure in matrix system and natural fracture system, respectively, Pa
p_i: Initial reservoir pressure, Pa
p_w: Wellbore pressure, Pa
q: Well rate, m^3/s
q^*: Mass flow velocity between matrix and fracture system in the reservoir of unit volume, $kg/(m^3 s)$
r: Radius, m
r_w: Well radius, m
S: Skin, dimensionless
t: Time, s
t_D: Dimensionless time, dimensionless
z: Laplace variable, dimensionless
α: Shape factor between matrix and fracture, m^{-2}
ρ_m, ρ_f: Oil density at pressure p_m in the matrix system and at pressure p_f in natural fracture system, respectively, kg/m^3
ρ_o: Oil density under initial condition, kg/m^3
γ: Permeability modulus, Pa^{-1}
γ_D: Dimensionless permeability modulus, dimensionless
λ: Dimensionless interporosity flow coefficient, dimensionless
ω: Storage ratio, dimensionless
μ: Viscosity of oil, Pa•s
φ_m, φ_f: Porosity of matrix and natural fracture system, respectively, fraction
φ_{mi}, φ_{fi}: Porosity of matrix and natural fracture system under initial condition, respectively, fraction
v_m, v_f: Flow velocity of fluid in matrix and natural fracture system, respectively, m/s.

Superscripts

-: Laplace transformation.

Subscripts

D: Dimensionless
m: Matrix
f: Fracture
w: Well.

Abbreviations

EOB: Elastic outer boundary
DPR: Dual-porosity reservoir
SSP: Stress sensitivity of permeability
PPD: Pressure and pressure derivative.

Data Availability

The data used to support the findings of this study are included within the article.

Conflicts of Interest

The authors declare that they have no conflicts of interest.

Acknowledgments

We gratefully acknowledge all professors of the Petroleum Institute, Faculty of Earth Science and Technology, Kim Chaek University of Technology, for their valuable suggestions and discussions. This study was supported by the National Science and Technical Development Foundation of DPR Korea (Grant no. 02017548–455).

References

[1] L. Wang, S. Yang, Z. Meng et al., "Time-dependent shape factors for fractured reservoir simulation: effect of stress sensitivity in matrix system," *Journal of Petroleum Science and Engineering*, vol. 163, pp. 556–569, 2018.

[2] Z. Zhang, S. He, D. Gu, S. Gai, and G. Li, "Effects of stress-dependent permeability on well performance of ultra-low permeability oil reservoir in China," *Journal of Petroleum Exploration and Production Technology*, vol. 8, no. 2, pp. 565–575, 2018.

[3] Y. Shu and J. Yan, "Characterization and prevention of formation damage for fractured carbonate reservoir formations with low permeability," *Petroleum Science*, vol. 5, no. 4, pp. 326–333, 2008.

[4] A. P. S. Selvadurai, D. Zhang, and Y. Kang, "Permeability evolution in natural fractures and their potential influence on loss of productivity in ultra-deep gas reservoirs of the Tarim Basin, China," *Journal of Natural Gas Science and Engineering*, vol. 58, pp. 162–177, 2018.

[5] R. Wang, X. Yue, R. Zhao, P. Yan, and D. Freeman, "Effect of stress sensitivity on displacement efficiency in CO_2 flooding for fractured low permeability reservoirs," *Petroleum Science*, vol. 6, no. 3, pp. 277–283, 2009.

[6] Y. Feng, Y. Liu, and G. Lei, "Study on stress-dependent permeability of fracture networks in fractured porous media," *Geofluids*, vol. 2021, Article ID 7433547, 19 pages, 2021.

[7] X. Tian, L. Cheng, W. Zhao, Y. Yan, X. He, and Q. Guo, "Experimental study on permeability stress sensitivity in tight sandstone oil reservoirs," *Sains Malaysiana*, vol. 44, no. 5, pp. 719–725, 2015.

[8] S. Zheng, "The research on the pressure sensitivity for low permeability fractured CBM reservoir," *International Journal of Earth Sciences and Engineering*, vol. 8, no. 2, pp. 9–13, 2015.

[9] Y. Yang, X. Peng, and X. Liu, "The stress sensitivity of coal bed methane wells and impact on production," *Procedia Engineering*, vol. 31, pp. 571–579, 2012.

[10] J. Shi, S. Wang, K. Wang, C. Liu, S. Wu, and K. Sepehrnoori, "An accurate method for permeability evaluation of undersaturated coalbed methane reservoirs using early dewatering data," *International Journal of Coal Geology*, vol. 202, pp. 147–160, 2019.

[11] J. Zhang, C. Wei, W. Ju et al., "Stress sensitivity characterization and heterogeneous variation of the pore- fracture system in middle-high rank coals reservoir based on NMR experiments," *Fuel*, vol. 238, pp. 331–344, 2019.

[12] G. V. Chilingar, H. H. Rieke, and A. F. Al-Anazi, "Why many overpressured, stress-sensitive hydrocarbon reservoirs should not be abandoned," *Energy Sources, Part A: Recovery, Utilization, and Environmental Effects*, vol. 27, no. 16, pp. 1495–1501, 2005.

[13] J. Guo, F. Meng, A. Jia et al., "Production behavior evaluation on multilayer commingled stress-sensitive carbonate gas reservoir," *Energy Exploration & Exploitation*, vol. 39, no. 1, pp. 86–107, 2021.

[14] F. Meng, Q. Lei, D. He et al., "Production performance analysis for deviated wells in composite carbonate gas reservoirs," *Journal of Natural Gas Science and Engineering*, vol. 56, pp. 333–343, 2018.

[15] R. Aguilera, "Effect of fracture compressibility on gas-in-place calculations of stress-sensitive naturally fractured reservoirs," *SPE Reservoir Evaluation & Engineering*, vol. 11, no. 2, pp. 307–310, 2008.

[16] Z. Wang, B. Ran, M. Tong, C. Wang, and Q. Yue, "Forecast of fractured horizontal well productivity in dual permeability layers in volcanic gas reservoirs," *Petroleum Exploration and Development*, vol. 41, no. 5, pp. 642–647, 2014.

[17] J. Wang, A. Jia, Y. Wei, and Y. Qi, "Approximate semi-analytical modeling of transient behavior of horizontal well intercepted by multiple pressure-dependent conductivity fractures in pressure-sensitive reservoir," *Journal of Petroleum Science and Engineering*, vol. 153, pp. 157–177, 2017.

[18] A. Luo, Y. Li, L. Wu, Y. Peng, and W. Tang, "Fractured horizontal well productivity model for shale gas considering stress sensitivity, hydraulic fracture azimuth, and interference between fractures," *Natural Gas Industry B*, vol. 8, no. 3, pp. 278–286, 2021.

[19] S. Mo, S. He, G. Lei, and S. Gai, "Deliverability equation in pseudo-steady state for fractured vertical well in tight gas," *Journal of Petroleum Exploration and Production Technology*, vol. 6, no. 1, pp. 33–38, 2016.

[20] L.-H. Zhang, J.-J. Guo, and Q.-G. Liu, "A new well test model for stress-sensitive and radially heterogeneous dual-porosity reservoirs with non-uniform thicknesses," *Journal of Hydrodynamics*, vol. 23, no. 6, pp. 759–766, 2011.

[21] L. Tian, K. Zhang, G. Liu, and J. Guo, "A well testing model on pressure characteristics of the heterogeneous composite gas reservoir," *GeoConvention*, vol. 2017, pp. 1–10, 2017.

[22] J. Ren and P. Guo, "A general analytical method for transient flow rate with the stress-sensitive effect," *Journal of Hydrology*, vol. 565, pp. 262–275, 2018.

[23] T. A. Jelmert and T. Toverud, "Compaction in a confined deforming reservoir," *Energy Procedia*, vol. 128, pp. 165–171, 2017.

[24] D. Xia, Z. Yang, D. Li, Y. Zhang, X. Zhao, and L. Yao, "Research on numerical method for evaluation of vertical well volume fracturing effect based on production data and well test data," *Journal of Petroleum Exploration and Production*, vol. 11, no. 4, pp. 1855–1863, 2021.

[25] Q. Zhu and H. Liang, "Productivity analysis method of abnormal high-pressure gas reservoir in Ying-Qiong Basin," *Natural Resources*, vol. 8, no. 6, pp. 410–415, 2017.

[26] M. Moradi, A. Shamloo, M. Asadbegi, and A. D. Dezfuli, "Three dimensional pressure transient behavior study in stress sensitive reservoirs," *Journal of Petroleum Science and Engineering*, vol. 152, pp. 204–211, 2017.

[27] H. Zhu, X. Tang, Q. Liu et al., "Permeability stress-sensitivity in 4D flow-geomechanical coupling of Shouyang CBM reservoir, Qinshui Basin, China," *Fuel*, vol. 232, pp. 817–832, 2018.

[28] Z. Li, Z. Qi, W. Yan et al., "Prediction of production performance of refractured shale gas well considering coupled multiscale gas flow and geomechanics," *Geofluids*, vol. 2020, Article ID 9160346, 21 pages, 2020.

[29] J. Chen, X. Song, B. Li, W. Li, C. Liao, and L. Yang, "Mathematical simulation about gas transport in a dual-porosity tight gas reservoir considering multiple effects," *Geofluids*, vol. 2021, Article ID 7483445, 7 pages, 2021.

[30] Y. Xue, Q. Jin, and H. Tian, "Productivity Influence factors of tight sandstone gas reservoir with water produced," *Geofluids*, vol. 2021, Article ID 9926299, 9 pages, 2021.

[31] L. Zhao, Z. Fan, M. Wang et al., "Productivity evaluation of vertical wells incorporating fracture closure and reservoir pressure drop in fractured reservoirs," *Mathematical Problems in Engineering*, vol. 2020, Article ID 9356178, 11 pages, 2020.

[32] H. Jabbari, Z. Zeng, S. F. Korom, and M. Khavanin, "Well test analysis in dual-porosity aquifers with stress-dependent conductivity," *Research Journal of Environmental and Earth Sciences*, vol. 4, no. 11, pp. 962–981, 2012.

[33] V. F. Samaniego and L. H. Villalobos, "Transient pressure analysis of pressure-dependent naturally fractured reservoirs," *Journal of Petroleum Science and Engineering*, vol. 39, no. 1-2, pp. 45–56, 2003.

[34] Z. Zhang, S. He, G. Liu, X. Guo, and S. Mo, "Pressure buildup behavior of vertically fractured wells with stress-sensitive conductivity," *Journal of Petroleum Science and Engineering*, vol. 122, pp. 48–55, 2014.

[35] L. Wang and X. Wang, "Modelling of pressure transient behaviour for fractured gas wells under stress-sensitive and slippage effects," *International Journal of Oil, Gas and Coal Technology*, vol. 11, no. 1, pp. 18–38, 2016.

[36] Y. Huang, X. Li, and X. Tan, "Transient pressure and rate decline analysis for horizontal well in stress-sensitive composite reservoir," *Mathematical Problems in Engineering*, vol. 2018, Article ID 8672578, 11 pages, 2018.

[37] X.-P. Li, L.-N. Cao, C. Luo, B. Zhang, J.-Q. Zhang, and X.-H. Tan, "Characteristics of transient production rate performance of horizontal well in fractured tight gas reservoirs with stress-sensitivity effect," *Journal of Petroleum Science and Engineering*, vol. 158, pp. 92–106, 2017.

[38] B. Yuan, C. R. Clarlson, Z. Zhang, and X. Zhu, "Deviations from transient linear flow behavior: A systematic investigation of possible controls on abnormal reservoir signatures," *Journal of Petroleum Science and Engineering*, vol. 205, article 108910, 2021.

[39] Z. Li, X. Wu, G. Han et al., "Transient pressure analysis of volume-fractured horizontal wells considering complex fracture networks and stress sensitivity in tight reservoirs," *ACS Omega*, vol. 4, no. 11, pp. 14466–14477, 2019.

[40] H. Wang, Q. Ran, and X. Liao, "Pressure transient responses study on the hydraulic volume fracturing vertical well in

stress-sensitive tight hydrocarbon reservoirs," *International Journal of Hydrogen Energy*, vol. 42, no. 29, pp. 18343–18349, 2017.

[41] J. Jiang and J. Yang, "Coupled fluid flow and geomechanics modeling of stress-sensitive production behavior in fractured shale gas reservoirs," *International Journal of Rock Mechanics and Mining Sciences*, vol. 101, pp. 1–12, 2018.

[42] C. Guo, J. Xu, M. Wei, and R. Jiang, "Pressure transient and rate decline analysis for hydraulic fractured vertical wells with finite conductivity in shale gas reservoirs," *Journal of Petroleum Exploration and Production Technology*, vol. 5, no. 4, pp. 435–443, 2015.

[43] M. Wu, M. Ding, J. Yao, S. Xu, L. Li, and X. Li, "Pressure transient analysis of multiple fractured horizontal well in composite shale gas reservoirs by boundary element method," *Journal of Petroleum Science and Engineering*, vol. 162, pp. 84–101, 2018.

[44] Y. Xu, X. Li, Q. Lin, and X. Tan, "Pressure performance of multi-stage fractured horizontal well considering stress sensitivity and dual permeability in fractured gas reservoir," *Journal of Petroleum Science and Engineering*, vol. 201, article 108154, 2021.

[45] Y. Zhang and D. Yang, "Modeling transient pressure behaviour of a multi-fractured horizontal well in a reservoir with an arbitrary boundary and different fracture networks by considering stress-sensitive effect," *Journal of Hydrology*, vol. 600, article 126552, 2021.

[46] Y. Zhang and D. Yang, "Evaluation of transient pressure responses of a hydraulically fractured horizontal well in a tight reservoir with an arbitrary shape by considering stress-sensitive effect," *Journal of Petroleum Science and Engineering*, vol. 202, article 108518, 2021.

[47] R. Zongxiao, W. Xiaodong, H. Guoqing et al., "Transient pressure behavior of multi-stage fractured horizontal wells in stress-sensitive tight oil reservoirs," *Journal of Petroleum Science and Engineering*, vol. 157, pp. 1197–1208, 2017.

[48] Z. Wu, C. Cui, G. Lv, S. Bing, and G. Cao, "A multi-linear transient pressure model for multistage fractured horizontal well in tight oil reservoirs with considering threshold pressure gradient and stress sensitivity," *Journal of Petroleum Science and Engineering*, vol. 172, pp. 839–854, 2019.

[49] J. Ji, Y. Yao, S. Huang, X. Ma, S. Zhang, and F. Zhang, "Analytical model for production performance analysis of multi-fractured horizontal well in tight oil reservoirs," *Journal of Petroleum Science and Engineering*, vol. 158, pp. 380–397, 2017.

[50] S. Huang, Y. Yao, S. Zhang, J. Ji, and R. Ma, "Pressure transient analysis of multi-fractured horizontal wells in tight oil reservoirs with consideration of stress sensitivity," *Arabian Journal of Geosciences*, vol. 11, no. 11, p. 285, 2018.

[51] Z. Wu, C. Cui, Z. Wang, Y. Sui, P. Jia, and W. Tang, "Well testing model of multiple fractured horizontal well with consideration of stress-sensitivity and variable conductivity in tight gas reservoirs," *Mathematical Problems in Engineering*, vol. 2018, Article ID 1693184, 13 pages, 2018.

[52] G. Wang, A. Jia, Y. Wei, and C. Xiao, "Transient pressure analysis for multifractured horizontal well with the use of multi-linear flow model in shale gas reservoir," *Geofluids*, vol. 2020, Article ID 8348205, 20 pages, 2020.

[53] M. Liu, C. Xiao, Y. Wang et al., "Sensitivity analysis of geometry for multi-stage fractured horizontal wells with consideration of finite-conductivity fractures in shale gas reservoirs," *Journal of Natural Gas Science and Engineering*, vol. 22, pp. 182–195, 2015.

[54] D. Du, G. Zhang, Y. Zhao, X. Sun, and B. Zhang, "Transient flow theory of multiple-fractured horizontal wells with complex mechanisms in shale gas reservoirs," *Geofluids*, vol. 2020, Article ID 7364734, 17 pages, 2020.

[55] Z. Chen, X. Liao, X. Zhao, X. Dou, and L. Zhu, "A semi-analytical mathematical model for transient pressure behavior of multiple fractured vertical well in coal reservoirs incorporating with diffusion, adsorption, and stress-sensitivity," *Journal of Natural Gas Science and Engineering*, vol. 29, pp. 570–582, 2016.

[56] H. Wang, Z. Kou, J. Guo, and Z. Chen, "A semi-analytical model for the transient pressure behaviors of a multiple fractured well in a coal seam gas reservoir," *Journal of Petroleum Science and Engineering*, vol. 198, article 108159, 2021.

[57] H. Liu, "The numerical simulation for multistage fractured horizontal well in low-permeability reservoirs based on modified Darcy's equation," *Journal of Petroleum Exploration and Production Technology*, vol. 7, no. 3, pp. 735–746, 2017.

[58] L. Zhang, J. Guo, and Q. Liu, "A well test model for stress-sensitive and heterogeneous reservoirs with non-uniform thicknesses," *Petroleum Science*, vol. 7, no. 4, pp. 524–529, 2010.

[59] H. Wang, J. Guo, and L. Zhang, "A semi-analytical model for multilateral horizontal wells in low-permeability naturally fractured reservoirs," *Journal of Petroleum Science and Engineering*, vol. 149, pp. 564–578, 2017.

[60] C. Cao, L. Cheng, X. Zhang, and J. Shi, "Numerical simulation investigation on well performance integrated stress sensitivity and sand production," *Geofluids*, vol. 2021, Article ID 9925866, 11 pages, 2021.

[61] Z. Yan, C. Cao, M. Xie et al., "Pressure behavior analysis of permeability changes due to sand production in offshore loose sandstone reservoirs using boundary-element method," *Geofluids*, vol. 2021, Article ID 6658875, 10 pages, 2021.

[62] Y. G. Zhang and D. K. Tong, "The pressure transient analysis of deformation of fractal medium," *Journal of Hydrodynamics*, vol. 20, no. 3, pp. 306–313, 2008.

[63] Y. Gao, R. Jiang, X. Xu et al., "The pressure buildup well test analysis considering stress sensitivity effect for deepwater composite gas reservoir with high temperature and pressure," *Geofluids*, vol. 2021, Article ID 5054246, 16 pages, 2021.

[64] I. Shovkun and D. N. Espinoza, "Coupled fluid flow-geomechanics simulation in stress-sensitive coal and shale reservoirs: impact of desorption-induced stresses, shear failure, and fines migration," *Fuel*, vol. 195, pp. 260–272, 2017.

[65] S. Li, C. Zhao, P. Zheng, and Q. Gui, "Analysis of oil and gas flow characteristics in the reservoir with the elastic outer boundary," *Journal of Petroleum Science and Engineering*, vol. 175, pp. 280–285, 2019.

[66] S. Li, H. Guo, P. Zheng, X. Dong, C. Zhao, and Q. Gui, "The elastic boundary value problem of extended modified Bessel equation and its application in fractal homogeneous reservoir," *Computational and Applied Mathematics*, vol. 39, p. 63, 2020.

[67] S. C. Kim, C. G. Han, M. W. Rim, J. S. Kim, and M. J. Ryang, "Analyzing fluid flow characteristics in a dual-porosity reservoir with an elastic outer boundary," *Acta Geophysica*, vol. 69, no. 5, pp. 1843–1853, 2021.

[68] P. Zheng, Y. Zheng, S. Li, L. Leng, and X. Xia, "Analysis of flow characteristics of the dual media shale gas reservoir with the elastic outer boundary," *SN Applied Sciences*, vol. 3, no. 10, p. 800, 2021.

[69] C. Zhao and C. Min, "Analysis of the transient flow of non-Newtonian power-law fluids in homogeneous reservoirs with the elastic outer boundary," *Acta Geophysica*, vol. 69, no. 5, pp. 1865–1875, 2021.

[70] S. C. Kim, Y. I. Song, and C. G. Han, "Improved numerical inverse Laplace transformation to improve the accuracy of type curve for analyzing well-testing data," *Acta Geophysica*, vol. 69, no. 3, pp. 919–930, 2021.

[71] Z. Wang, J. Yao, and X. Diao, "Pressure-sensitive dual porosity medium well test interpretation and its application in Tahe oilfield," *Xinjiang Petroleum Geology*, vol. 28, no. 2, pp. 235–237, 2007, in Chinese.

[72] O. A. Pedrosa, "Pressure transient response in stress-sensitive formations," in *Paper presented at the SPE California Regional Meeting*, Oakland, CA, USA, April 1986.

[73] J. E. Warren and P. J. Root, "The behavior of naturally fractured reservoirs," *SPE Journal*, vol. 3, no. 3, pp. 245–255, 1963.